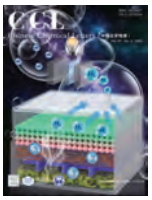
Chinese Chemical Letters 37 (2026) 111453

Contents lists available at ScienceDirect

Chinese Chemical Letters

journal homepage: www.elsevier.com/locate/cclet



An inverse opal structure-based human alveolar lung-on-a-chip for the study of Osimertinib treatment in non-small cell lung cancer

Weifei Zhang[a], Danfeng Xu[a], Jinru Tian[b], Ying Kan[a], Xuanlin Feng[a], Jia Liu[a], Hongmei Li[a,c,*], Nan Li[b,*]

[a] Key Laboratory of Chemical Metrology and Applications on Nutrition and Health, State Administration for Market Regulation, Division of Chemical Metroloy and Analytical Science, National Institute of Metrology, Beijing 100029, China
[b] School of Chinese Materia Medica, Beijing University of Chinese Medicine, Beijing 100029, China
[c] State Key Laboratory of Green Biomanufacturing College of Life Science and Technology, Beijing University of Chemical Technology, Beijing 100029, China

ARTICLE INFO

Article history:
Received 6 March 2025
Revised 12 June 2025
Accepted 12 June 2025
Available online 13 June 2025

Keywords:
Lung-on-a-chip
Inverse opal structure
Concentration gradient generator
Osimertinib metabolism
Adapted resistance
Amino acid metabolism

ABSTRACT

The deficiency of reliable and physiologically relevant distal lung models has been regarded as a crucial issue for drug research on non small cell lung cancer (NSCLC). In this study, an inverse opal structure-based lung-on-a-chip was established to replicate the geometric dimensions and topography of the native lung alveoli, and two lateral microchambers were designed to induce pressure-driven stretching for the simulation of respiratory movement. Further, a concentration gradient generator was applied to connect with lung-on-a-chip for the creation of different enzyme environments to mimic the individual variability of P450s enzymes in lung patients. Based on this microfluidic platform, the Osimertinib implications in NSLC was investigated from the aspect of metabolism and adapted resistance. The results suggested that Osimertinib exhibited discernible difference in metabolism under diverse enzyme condition. Additionally, in contrast with the control group, all groups with Osimertinib treatment triggered the alterations of amino acid metabolisms and energy supply, indicating that targeting energy supply process might be an effective measure to prevent tumor cells from generating drug resistance.

© 2026 Published by Elsevier B.V. on behalf of Chinese Chemical Society and Institute of Materia Medica, Chinese Academy of Medical Sciences.

In recent years, lung cancer has exhibited a sharp rise in both incidence and mortality, with non-small cell lung cancer (NSCLC) accounting for approximately 80 % of cases [1–3]. As a prevalent and lethal malignancy, NSCLC has been demonstrated to primarily localize to the bronchial and alveolar regions. The development of novel NSCLC therapeutics involves a prolonged timeline, spanning from target discovery through late-stage clinical trials to final regulatory approval. However, preclinical animal studies often fail to accurately predict outcomes in human trials, contributing to high attrition rates in drug development [4,5]. A critical bottleneck lies in the lack of physiologically relevant *in vitro* models replicating distal lung physiology, particularly alveolar microenvironments, which severely hampers drug discovery and mechanistic studies [6,7].

Microfluidic chips can provide cells with an environment that closely resembles native *in vivo* milieu, which is emerging as a promising tool for credible prediction [8–10]. Some classical micro-engineered microfluidic settings, named as first-generation lung-on-a-chip, integrated with a flexible porous polymeric membrane have been reported to model lung alveoli interfaces [11–14]. Despite a tremendous advance in mimicking the barrier tissue interfaces, these systems merely reflected alveoli's gross anatomy and were not able to reproduce a key biological aspect of the human lung [15]. The critical *in vivo* feature of lung alveoli is the array of tiny alveoli with physiological dimensions (reported to be around 100–200 μm). Indeed, the first-generation lung-on-a-chip could only create a single alveolus on the surface of the culturing membrane, imperfectly replicate the geometric dimensions and topography of the native lung alveoli.

Osimertinib, a third-generation EGFR-TKI, has transformed NSCLC treatment for EGFR-mutated patients but faces a critical limitation: >50 % develop resistance within 18 months, often leaving no effective therapies [16]. This challenge intensifies as its clinical use expands to first-line and adjuvant settings, exposing more patients to resistance risks. While genomic mechanisms are well-documented, emerging evidence implicates adaptive metabolic resistance, a transient survival phase enabling tumor cells to evade drug pressure while acquiring permanent mutations, as a pivotal but understudied precursor to therapeutic failure [17,18]. To some extent, progress in this field is hindered by owing to the lack of proper study model. It has been demonstrated that

* Corresponding authors.
E-mail addresses: lihm@buct.edu.cn (H. Li), linan@bucm.edu.cn (N. Li).

https://doi.org/10.1016/j.cclet.2025.111453
1001-8417/© 2026 Published by Elsevier B.V. on behalf of Chinese Chemical Society and Institute of Materia Medica, Chinese Academy of Medical Sciences.

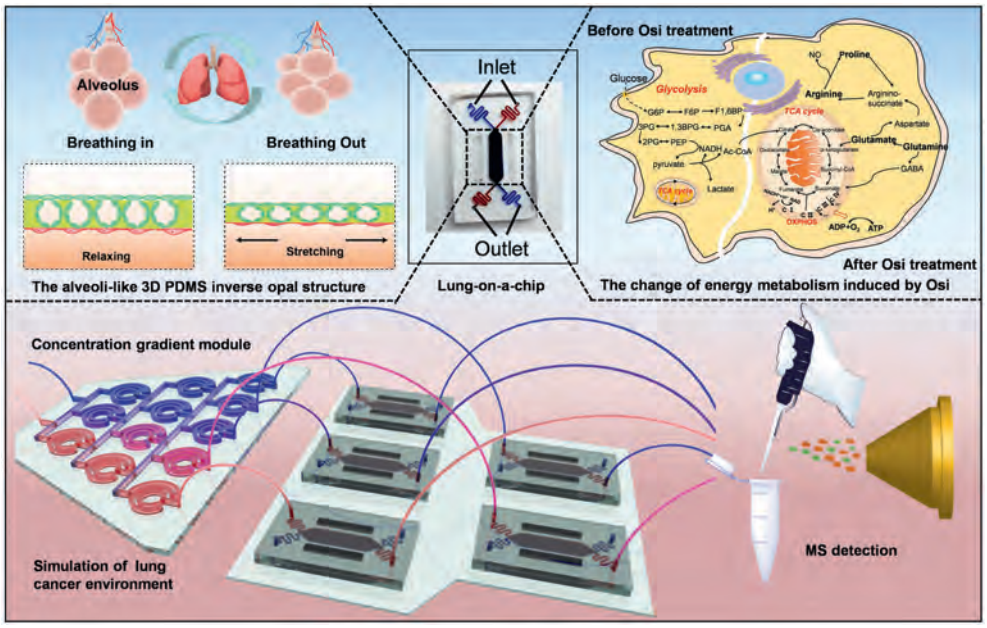


Fig. 1. Schematic diagram of the integrated device composed of lung-on-chip with alveolil-like 3D structures and concentration gradient module for the study of the metabolism and resistance induced by Osimertinib treatment in NSLC.

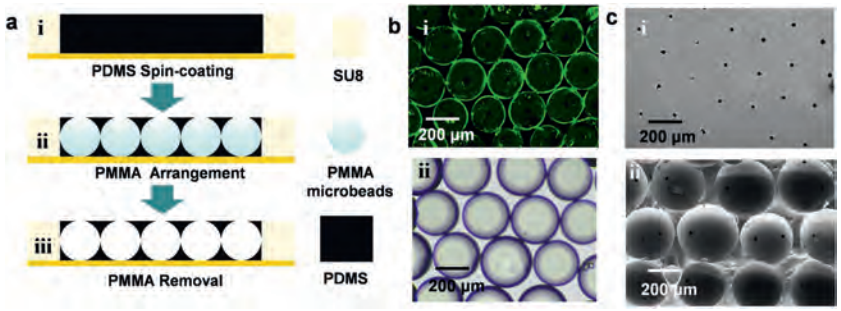


Fig. 2. The fabrication of alveoli-like 3D PDMS inverse opal structure. (a) Schematic diagram showed the fabrication procedure. (b) The fluorescence image (i) and brightfield image (ii) showed the alveoli-like structures. (c) SEM images exhibited both the apical and horizontal cross-section of this inverse opal structure.

Osimertinib metabolism hinged on cytochrome P450s enzymes (CYP450) activity [19,20]. CYP3A4 has been regarded as the major human enzyme responsible for Osimertinib metabolism in the liver, and CYP1A1-mediated metabolism has been considered to be of particular relevance to the treatment of lung cancer [20,21]. Human-relevant studies are further complicated by extreme inter-individual variability (>60-fold) in CYP450 expression due to polymorphisms, drug interactions, and tumor-induced paraneoplastic effects [22]. Therefore, developing engineered systems replicating human CYP450 crosstalk could unveil metabolic drivers of adaptive resistance, offering transformative insights into delaying or preventing acquired resistance, which was an urgent need given Osimertinib's expanding role across NSCLC stages.

To this end, in this study, we developed a human lung-on-chips with an array of alveoli-like three-dimensional (3D) and physiological dimensions for the study of Osimertinib metabolism and adaptive resistance in NSCLC. This model consisted of a 3D porous and stretchable polydimethylsiloxane (PDMS) featuring an inverse opal structure, bonded to a compartmentalized PDMS chip device. The inverse opal structures possessed uniform alveoli-like sacs with the interconnecting windows between them, which enabled the permeability and allowed cells to be cultured at the air-liquid interface. In addition, the elastic and biocompatible properties of PDMS allowed mimicking the dynamic respiration simulation by mechanically stretching the cells using vacuum chambers and air-pumping devices. The human lung adenocarcinoma cells (NCI-H1975, obtained from the BNCC Beijing, China) populated on the surfaces of the sacs were observed to form the monolayer for modeling the alveolar epithelium of NSCLC, and the lung alveoli air-blood barrier were reconstituted in combination with the human vascular endothelial cells (HUVECs, obtained from the BNCC Beijing, China) cultured on the bottom of the inverse opal PDMS structure. To investigate the Osimertinib metabolism in different enzyme composition of lung cancer, a concentration gradient generator was introduced to generate various enzyme environment with different concentration ratios of CYP3A4 and CYP1A1. The upsteam concentration gradient module and the downstream lung-on-a-chip was connected *via* polyethylene tubes. The integrated microfluidic device was an easy-to-use tool for the research of Osimertinib metabolism and adaptive resistance for NSCLC treatment (Fig. 1). This device would be promising to permit applications such as drug screening.

The typical procedure for the fabrication and characteristic of the alveoli-like 3D PDMS inverse opal structure was schematically presented in Fig. 2a. The PDMS prepolymer was spin coated on the template with grooves. Polymethyl methacrylate (PMMA) microbeads with a uniform diameter of 200 μm were placed in the groove by electrostatic adsorption, and assembled into a cubic close packed lattice. Keep still for a moment to make the PDMS prepolymers form a smooth surface, which was tangent with the

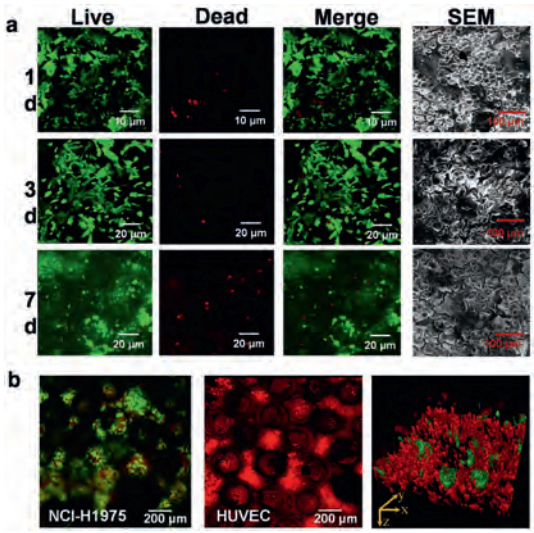


Fig. 3. Characteristic of the alveolar structure. (a) Fluorescence confocal images and SEM images showed the viability and morphology of alveolar epithelium at 1, 3, and 7 d. Green, live NCI-H1975 cells; red, dead NCI-H1975 cells. (b) Fluorescence confocal images showed the alveolar-like structure including both alveolar epithelium vascular endothelium. Green, live NCI-H1975 cells; red, live HUVECs.

top of PMMA microbeads. Then place this model at 65 °C for cross-link. Finally, an alveoli-like 3D PDMS with uniform pores and interconnecting windows between sacs were fabricated after removing the PMMA microbeads with tetrahydrofuran. This PDMS inverse opal structure was characterized by fluorescence microscopy (FM) and scanning electron microscopy (SEM). Taking advantage of the inherent property of PDMS in the aspect of high adsorption levels, a small molecule fluorescence dye, fluorescein isothiocyanate (FITC), was applied to illustrate these inverse opal structures based on the adsorption of the dye on the surface of the vesicle. The fluorescence images showed that these sacs closely assembled and the intersections were observed between most, if not all, of the adjacent sacs, and the bright-field optical image also displayed their structures (Fig. 2b). Further, the SEM images exhibited both the apical surface and horizontal cross-section of this PDMS inverse opal structure (Fig. 2c). An array of uniform pores with a diameter of 10 μm was observed on the PDMS structure surface. As for the horizontal cross-section, the tightly packed sac-like structures (about 200 μm diameters) with interconnecting windows between two adjacent sacs were observed, verifying the successful fabrication of PDMS inverse opal structure. Such structures replicated the miniature alveolar lung model, which mimicked the native human counterpart in both architecture and dimensions.

The schematic diagram of the human alveolar lung-on-a-chip device was shown in Fig. S1a (Supporting information), and the device was fabricated using a method previously developed by our

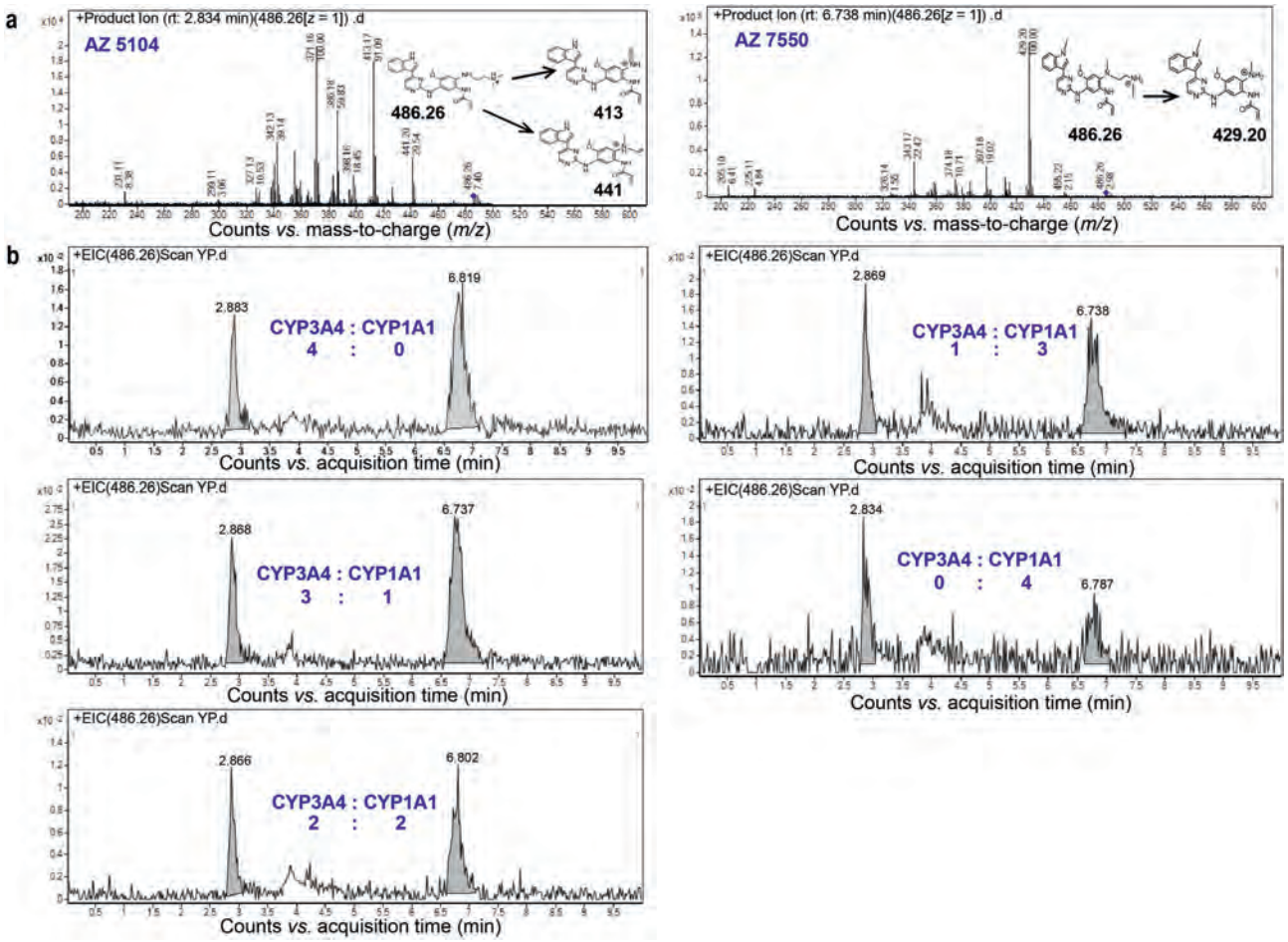


Fig. 4. Investigation of Osimertinib metabolism using LC/MS-MS. (a) Metabolite identification. MS/MS spectra and corresponding fragment schemes showed two demethylated metabolites, AZ5104 and AZ7550, with the same RT as the standard. (b) Comparison of Osimertinib metabolites generated in different proportion of CYP3A4 and CYP1A1 exposure levels.

group [23,24]. The intervening 3D PDMS inverse opal structure scaffold was bonded to two closely apposed PDMS microchannels, and two lateral microchambers were incorporated into the device to produce pressure-driven stretching for the simulation of respiratory movement. The device principle for simulating respiratory pneumatic was provided in Fig. S1b (Supporting information), and pressure-driven stretching was shown in Movie S1 (Supporting information). To form the alveolar epithelium of NSCLC model, NCI-H1975 were firstly populated on the apical surface of the PDMS inverse opal structures, after a period of growth, these cells gradually migrated from the surface micropores to the hollow sacs inside. The viability, spreading, and proliferation of the cells were indicated by live (green)/dead (red) dye, which verified the biocompatibility of this PDMS inverse opal structures. As shown in Fig. 3a, fluorescence images exhibited that the NCI-H1975 cells were relatively rounded after inoculation on the surface, followed by the spreading and proliferation at day 3 postseeding, and eventually, most cells transferred into sacs and covered the inner surface to form an alveolar-like structure at day 7 postseeding. Furthermore, the morphologies of NCI-H1975 were observed by SEM images, and the results suggested that a well-spread, relatively smooth, and confluent epithelium could be replicate with the increasing the culture period. For the creation of alveoli air-blood barrier, the lung-on-a-chip device was flipped, and HUVECs were seeded on the basal side of the inverse opal structure to reach confluence for the coculture. Celltracker green (NCI-H1975) and Celltracker deep red (HUVECs) staining provided an overview of alveolar-like structure, showing the distribution of both epithelial and endothelial cells (Fig. 3b).

To mimic Osimertinib metabolism in different enzyme composition, Osimertinib solution mixed separately with CYP3A4 and CYP1A1 were injected into the two inlets of a concentration gradient generator, which was developed based on the previous research [25,26]. Theoretically, the mixed enzyme concentration in the outlets was 4:0, 3:1, 2:2, 1:3, 0:4 (CYP3A4:CYP1A1) from left to right. The lung-on-a-chip connected to the concentration gradient module was used to investigate the difference of Osimertinib metabolism in lung cancer. Two demethylated metabolites (nanomolar levels) were identified including AZ5104 and AZ7550, and the metabolites were determined based on the retention time (RT) (Fig. S2 in Supporting information) and the characteristic MS/MS fragmentation (Fig. 4a). There were significant differences in Osimertinib metabolites between five groups. The lung-on-chip connected to the outlet containing only CYP3A4 exhibited high activity in the generation of AZ5104, AZ7550, while the lung-on-chip flowed through only CYP1A1 was active in generating AZ5104 (Fig. 4b). The variable relative abundance in the lung-on-chips was caused by the variability in CYP3A4 and CYP1A1 exposure levels. These results were basically coincident with the previous research [19], that CYP3A4 was primarily responsible for the generation and further metabolism of the key active metabolites AZ5104, AZ7550, and that CYP1A1 was highly active in generating AZ5104.

Having mimicked the Osimertinib metabolism in the different proportion of CYP3A4 and CYP1A1 exposure levels, the alterations of cell metabolites was further investigated. Metabolic reprogramming has been verified to be the molecular hallmark of cancer, and some evidence even suggested that metabolic reprogramming could mediate the development of acquired drug resistance in tumor cells [18]. The untargeted analysis between adaptive-resistant cells (after exposure for 72 h) and parental cells (0 h) was performed by metabolomics profiling. To assess the global metabolism variations, a supervised PLS-DA was performed in adapted cells (Samples 1–5) and parental cells (control) including both positive and negative spectra (Fig. S3 in Supporting information), followed by screening the differential metabolites. 33 metabolites were identified and the heatmap was shown in Fig. 5a, which in-

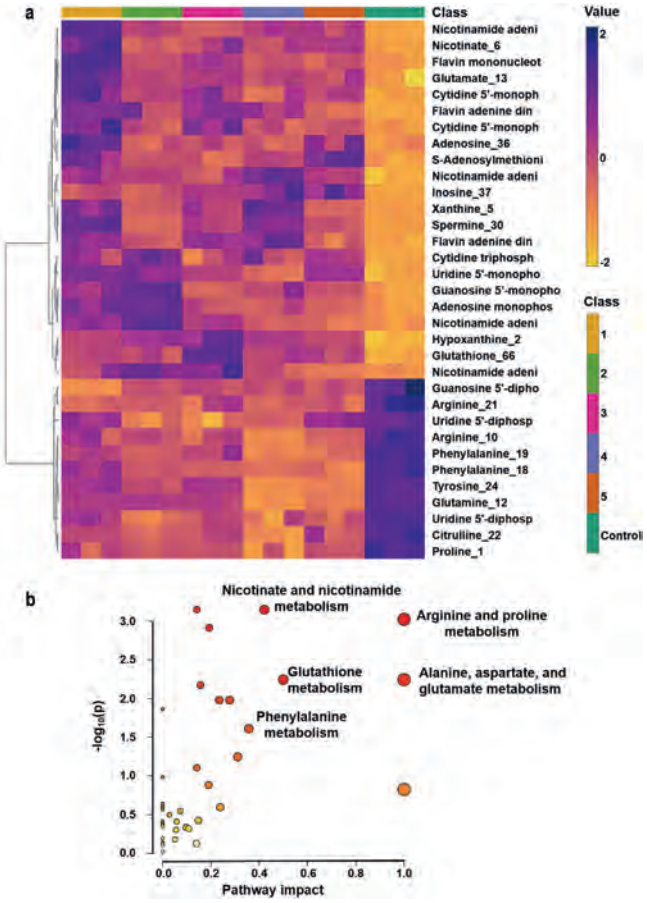


Fig. 5. Differential metabolites and corresponding pathways. (a) Heatmap of the intensities of differential metabolites in adaptive-resistant cells and parental cells ($n = 3$). The degree of change was marked with different colors: yellow indicated downregulation, and violet indicated upregulation. Each column represented an individual sample, and each row represented a metabolite. (b) Metabolism pathways participating in Osimertinib adapted resistance.

dicated that Osimertinib resistance was related to the amino acid metabolisms. The relevant biological pathways were analyzed by MetaboAnalyst, and the results showed that Osimertinib resistance was correlated with arginine and proline metabolism, glutathione metabolism, and alanine, aspartate, and glutamate metabolism (Fig. 5b). Continuously decreased glutamine levels were observed in adapted cells. This phenomenon was probably caused by the conversion of glutamine to glutamate *via* glutaminolysis, because drug-induced stress could affect energy production metabolism and the glutaminolysis contributed to the tricarboxylic acid (TCA) cycle for energy production based on the previous research [17]. The arginine and proline metabolism showed a down-regulated trend in adapted cells. A previous study regarded arginine as a major source for the synthesis of NO, proline and other metabolites. Among them, NO played a crucial role in the regulation of cancer progression, in which a low level of NO promoted cancer cells proliferation and inhibited apoptosis, while a high concentration of NO suppressed cell proliferation and facilitated cell apoptosis [27]. Thus, to a certain extent, a decreased of arginine and proline concentration in the adapted cells might suggest that Osimertinib resistance triggered a relatively active cell state. Moreover, some metabolites such as flavin adenine dinucleotide (FAD), nicotinamide adenine dinucleotide (NAD), flavin mononucleotide (FMN) in the oxidative phosphorylation (OXPHOS) were observed to be elevated in adapted cells, illustrating a significant alteration of OXPHOS in Osimertinib resistance cells. Based on these results, we

speculated that tumor cells would regulate their energy consumption patterns to resist severe conditions caused by cancer treatment.

In conclusion, we reconstructed a lung-on-a-chip integrated with a concentration gradient generator to model the pathological microenvironment for studying Osimertinib resistance in NSCLC. The chip featured an inverse opal structure mimicking alveolar geometry and pressure-driven respiratory motion, enabling reproducible fabrication for both research and scalable applications. Using this model, we uncovered that Osimertinib metabolism varied significantly with enzyme composition, while differential metabolite analysis linked resistance to dysregulated amino acid and energy metabolism, suggesting energy pathway targeting as a potential therapeutic strategy. Besides, this platform was able to simulate human-specific CYP450 activity and metabolic heterogeneity, allowing screening of drug candidates under physiologically relevant conditions, accelerating the development of resistance-breaking approach. However, our current studies used immortalized cell lines, in the future work, we will try to employ patient-derived organoids to predict individual responses to Osimertinib or combination therapies, which will hold transformative potential for personalized medicine and precision drug development. This evolution could bridge preclinical testing and clinical trials, reducing attrition rates in oncology drug development. By recapitulating interpatient variability in metabolism and resistance mechanisms, this platform may ultimately serve as a promising tool for stratifying NSCLC patients and optimizing therapeutic outcomes.

Declaration of competing interest

The authors declare that they have no known competing financial interest or personal relationships that could have appeared to influence the work reported in this paper.

CRediT authorship contribution statement

Weifei Zhang: Writing – review & editing, Writing – original draft, Methodology, Formal analysis, Data curation, Conceptualization. **Danfeng Xu:** Validation, Formal analysis, Data curation. **Jinru Tian:** Formal analysis, Data curation. **Ying Kan:** Writing – review & editing. **Xuanlin Feng:** Software, Methodology. **Jia Liu:** Investigation. **Hongmei Li:** Resources, Funding acquisition, Formal analysis. **Nan Li:** Writing – review & editing, Writing – original draft, Supervision, Resources, Project administration, Funding acquisition, Formal analysis, Conceptualization.

Acknowledgments

This work was supported by the National Key R&D Program of China (No. 2021YFF0600705), National Natural Science Foundation of China (Nos. 22204155 and 82404857) and the National Institute of Metrology Fundamental Research Project (No. AKYJJ2302), and the Fundamental Research Funds for the Central Universities (No. 2022-JYB-JBZR-018).

Supplementary materials

Supplementary material associated with this article can be found, in the online version, at doi:10.1016/j.cclet.2025.111453.

References

[1] D.F. Heigener, M. Reck, Nat. Rev. Clin. Oncol. 15 (2018) 71–72.
[2] H. Wang, Q. Hu, Y. Chen, et al., Nat. Commun. 15 (2024) 4195.
[3] H. Lu, J. Ye, Y. Wei, et al., Chin. Chem. Lett. 36 (2025) 110077.
[4] L. Ma, N. Li, J. Wang, et al., TrAC Trends Anal. Chem. 160 (2023) 116951.
[5] D. Huang, T. Liu, J. Liao, et al., Proc. Natl. Acad. Sci. U. S. A. 118 (2021) e2016146118.
[6] P.N. Fonkwo, EMBO Rep. 9 (2008) S13–S17.
[7] E. Purev, K. Bahmed, B. Kosmider, Biomolecules 14 (2024) 115.
[8] N. Li, W.F. Zhang, Y.X. Li, J.M. Lin, TrAC Trends Anal. Chem. 117 (2019) 200–214.
[9] S. Jiang, Y. Kan, B.F. Zhu, H.M. Li, W.F. Zhang, Chin. J. Anal. Lab. 44 (2025) 133–147.
[10] N. Li, W.F. Zhang, L. Lin, et al., Chem. Commun. 54 (2018) 11435–11438.
[11] D. Huh, B.D. Matthews, A. Mammoto, et al., Science 328 (2010) 1662–1668.
[12] D. Huh, H. Fujioka, Y.C. Tung, et al., Proc. Natl. Acad. Sci. U. S. A. 104 (2007) 18886–18891.
[13] A.O. Stucki, J.D. Stucki, S.R.R. Hall, et al., Lab Chip 15 (2015) 1302–1310.
[14] K.H. Benam, R. Villenave, C. Lucchesi, et al., Nat. Methods 13 (2016) 151–157.
[15] P. Zamprogno, S. Wüthrich, S. Achenbach, et al., Commun. Biol. 4 (2021) 168.
[16] X. Hu, Q. Xun, T. Zhang, et al., Chin. Chem. Lett. 31 (2020) 1281–1287.
[17] X. Han, D. Wang, L. Yang, et al., Proc. Natl. Acad. Sci. U. S. A. 121 (2024) e2319429121.
[18] M. Nie, N. Chen, H. Pang, et al., J. Clin. Invest. 132 (2022) e160152.
[19] A.K. MacLeod, D. Lin, J.T. Huang, et al., Clin. Cancer Res. 24 (2018) 2138–2147.
[20] P.A. Dickinson, M.V. Cantarini, J. Collier, et al., Drug Metab. Dispos. 44 (2016) 1201–1212.
[21] T.L. McLemore, S. Adelberg, M.C. Liu, et al., J. Natl. Cancer Inst. 82 (1990) 1333–1339.
[22] L.M. Forrester, C.J. Henderson, M.J. Glancey, et al., Biochem. J. 281 (1992) 359–368.
[23] N. Li, W.F. Zhang, M. Khan, L. Lin, J.M. Lin, Biosens. Bioelectron. 99 (2018) 142–149.
[24] W.F. Zhang, N. Li, L. Lin, et al., Small 16 (2020) 1903402.
[25] D. Gao, H. Li, N. Wang, J.M. Lin, Anal. Chem. 84 (2012) 9230–9237.
[26] X. Liu, Y. Jia, Z. Han, et al., Angew. Chem. Int. Ed. 60 (2021) 12319–12322.
[27] R. Keshet, A. Erez, Dis. Model Mech. 11 (2018) dmm033332.